Journal of Computational Acoustics

A FOURIER COLLOCATION APPROACH FOR TRANSIT-TIME ULTRASONIC FLOWMETER UNDER MULTI-PHASE FLOW CONDITIONS

MATEJ SIMURDA
Mads Clausen Institute, University of Southern Denmark, Sønderborg, 6400, Denmark
simurda@mci.sdu.dk

BENNY LASSEN
Mads Clausen Institute, University of Southern Denmark, Sønderborg, 6400, Denmark

LARS DUGGEN
Mads Clausen Institute, University of Southern Denmark, Sønderborg, 6400, Denmark

NILS T. BASSE
[2]*Siemens A/S Flow Instruments, Sønderborg, 6400, Denmark*

Received (Day Month Year)
Revised (Day Month Year)

A numerical model for a clamp-on transit-time ultrasonic flowmeter (TTUF) under multi-phase flow conditions is presented. The method solves equations of linear elasticity for isotropic heterogeneous materials with background flow where acoustic media are modelled by setting shear modulus to zero. Spatial derivatives are calculated by a Fourier collocation method allowing the use of the fast Fourier transform and time derivatives are approximated by a finite difference scheme. This approach is sometimes referred to as a pseudospectral time-domain method. Perfectly matched layers are used to avoid wave-wrapping and staggered grids are implemented to improve stability and efficiency. The method is verified against exact analytical solutions and the effect of the time-staggering and associated lowest number of points per minimum wavelengths value is discussed. The method is then employed to model a complete TTUF measurement setup to simulate the effect of a flow profile on the flowmeter accuracy and a study of an impact of inclusions in flowing media on received signals is carried out.

Keywords: Fourier collocation; Ultrasonic propagation ; Flow measurement; Two-phase flow; Elasticity

1. Introduction

Transit-time ultrasonic flowmeters (TTUF) are devices that enable noninvasive fluid flow rate measurement based on difference of times it takes an ultrasonic beam to cross the pipe

when propagating with and against the flow. They can be either mounted directly into a pipeline or clamped-on from the outside. Moreover, flowing media can consist of two or more substances so the ultrasonic beam has to cross multiple solid-solid, solid-fluid and fluid-fluid interfaces. This affects the measurement signal significantly and it is not trivial to derive an analytical model for such setups. There have been several approaches published to this problem among the more commonly used are ray-tracing algorithms[1,2] which, however do not account for diffraction, or finite difference (FD)[3] and finite element methods (FEM)[4] where the wave theory is employed through solving the linearized Euler equations (acoustic media) or the equations of linear elasticity (solid media). These methods showed good results but suffer from high memory demands as they require a relatively high number of points per minimum wavelengths (PPMW). An alternative approach was presented by Bezdek *et al.*[5] where FEM is only used in the solid parts and a boundary integral method is applied in the fluid. Such approach reduces the computational complexity but assumes that the flowing fluid is homogeneous.

In this paper we demonstrate an alternative approach called a pseudospectral time domain (PSTD)[6] method. Spatial derivatives are calculated using the Fourier collocation method that reduces the PPMW value and allows the use of the fast Fourier transform (FFT). Temporal integration is realized by the explicit Euler central finite difference scheme for quiescent media and the third order Adams-Bashforth (AB3) method[8] for media with background flow. First, the PSTD method is verified against analytical solutions and the benefits of using temporally and spatially staggered grids is discussed. Finally, a study of a complete ultrasonic flow meter setup and its accuracy for various flow conditions is presented.

2. Model of elastic/acoustic wave propagation

A lossless propagation of both elastic and acoustic waves in isotropic media can be modelled by a system of first order partial differential equations of linear elasticity that couple particle displacement velocity v_i and stress σ_{ij}[7]

$$\frac{\partial \sigma_{ij}}{\partial t} = \lambda \delta_{ij} \frac{\partial v_k}{\partial x_k} + \mu \left(\frac{\partial v_i}{\partial x_j} + \frac{\partial v_j}{\partial x_i} \right), \tag{1}$$

$$\rho \frac{\partial v_i}{\partial t} = \frac{\partial \sigma_{ij}}{\partial x_j} + f_i, \tag{2}$$

where f_i is the body force, x_i, $i = 1, 2, 3$ are Cartesian position coordinates and λ, μ and ρ denote the Lamé elastic constant, shear modulus and mass density respectively. In these equations the Einstein summation convention is used. For infinite homogeneous media, the material parameters are related to the compressional c_p and shear wave velocities c_s as

$$c_p = \sqrt{\frac{\lambda + 2\mu}{\rho}}, \qquad c_s = \sqrt{\frac{\mu}{\rho}}. \tag{3}$$

The acoustic media are modelled by setting the shear modulus μ to zero. Assuming a presence of background flow the governing equations become[9]

$$\frac{\partial \sigma_{ij}}{\partial t} = \lambda \delta_{ij} \frac{\partial v_k}{\partial x_k} + \mu \left(\frac{\partial v_i}{\partial x_j} + \frac{\partial v_j}{\partial x_i} \right) - \lambda \delta_{ij} v_{0k} \frac{\partial}{\partial x_k} \left(\frac{\sigma_{ij}}{\lambda} \right), \tag{4}$$

$$\rho \frac{\partial v_i}{\partial t} = \frac{\partial \sigma_{ij}}{\partial x_j} + f_i - \rho v_{0k} \frac{\partial v_i}{\partial x_k} - \rho v_k \frac{\partial v_{0i}}{\partial x_k}, \tag{5}$$

where v_{0i} is the background flow velocity allowed to vary arbitrarily in time and space but being zero in elastic media.

3. Numerical implementation

3.1. *Fourier collocation method*

Unlike the FEM, spectral methods use basis functions that are nonzero over the entire domain and therefore approximate spatial derivatives at each point globally. Consider an arbitrary interval of length l discretized into N evenly distributed points with step size Δx ($l = \Delta x N$). The Fourier collocation method calculates spatial derivative as[10]

$$\frac{\partial [.]}{\partial x} \approx Re \left(\mathcal{F}^{-1} \left(ik \mathcal{F}(.) \right) \right), \tag{6}$$

where $\mathcal{F}$ and $\mathcal{F}^{-1}$ denote the discrete Fourier and inverse Fourier transform of a function $f(x)$ respectively, in this work defined as

$$\begin{aligned} \mathcal{F}\left(f(x)\right)(k) = \hat{f}(k) &= \Delta x \sum_{j=1}^{N} f(x_j) e^{-ikx_j}, \\ \mathcal{F}^{-1}\left(\hat{f}(k)\right)(x) = f(x) &= \frac{1}{\Delta x N} \sum_{j=1}^{N} e^{-ik_j x} \hat{f}(k_j), \end{aligned} \tag{7}$$

and k is the vector of wavenumbers

$$k = \begin{cases} \left[-\frac{N}{2}, -\frac{N}{2} + 1, ..., \frac{N}{2} - 1 \right] \frac{2\pi}{\Delta x N} & \text{if } N \text{ is even} \\ \left[-\frac{N-1}{2}, -\frac{N-1}{2} + 1, ..., \frac{N-1}{2} - 1 \right] \frac{2\pi}{\Delta x N} & \text{if } N \text{ is odd} \end{cases} \tag{8}$$

This intuitively suggests that these methods will develop issues for problems with discontinuous parameters due to *Gibbs phenomenon* but as many studies already showed they often outperform local approaches such as the FEM and FD[11,12].

3.2. *Perfectly matched layers*

The trigonometric interpolation used by the Fourier collocation inherently imposes periodic boundary conditions. These cause waves leaving the domain on one side to instantly reappear on the opposite side which is sometimes called wave-wrapping[12]. In this paper, we suppress this issue by implementing perfectly matched layers (PML). This adds an extra non-physical absorbing boundary layer around the domain of interest where all waves are damped. One drawback is that this method requires all velocity and stress fields to be artificially split into components associated with only one spatial coordinate which increases the number of unknowns by factor of two (2D) or three (3D) as the equations (4) and (5) are modified as follows[13]

$$\frac{\partial_l \sigma_{mn}}{\partial t} = \lambda \delta_{mn} \frac{\partial v_l}{\partial x_l} + \mu \left(\delta_{nl} \frac{\partial v_m}{\partial x_l} + \delta_{ml} \frac{\partial v_n}{\partial x_l} \right) - \lambda \delta_{mn} v_{0l} \frac{\partial}{\partial x_l} \left(\frac{\sigma_{mn}}{\lambda} \right) - G_l \sigma_{mn}, \tag{9}$$

$$\frac{\partial_l v_m}{\partial t} = \frac{1}{\rho} \frac{\partial \sigma_{lm}}{\partial x_l} + \frac{1}{\rho} \delta_{lm} f_m - v_{0l} \frac{\partial v_m}{\partial x_l} - v_m \frac{\partial v_{0m}}{\partial x_l} - G_l v_m, \tag{10}$$

where $l, m, n = x, y, z$. Note that the summation convention is not used in (9) and (10) so the terms associated with different spatial derivatives are separated. G_l is the damping parameter, in this work defined as

$$G_l = A(x_l - x_{l0})^n, \tag{11}$$

where x_{l0} is the coordinate at the inner edge of the PML. The specific values of magnitude A and order n have been chosen experimentally so the wave amplitudes at the periodic boundaries get attenuated to the order of computational precision. It has been shown that the convective terms together with the PML make rise to some unstable wave modes that grow exponentially in the PML region[14]. Many works have been published where alternative representation of the PML is given that is stable for homogeneous background flow even in an arbitrary direction[15] but there is no equivalently simple representation of such absorbing layers for acoustic wave equation with inhomogeneous background flow. It has been however found experimentally during this work that imposing multi-axial perfectly matched layers (M-PML)[16] suppresses these instabilities.

$$G_l = A(x_l - x_{l0})^n + Ar(1 - \delta_{lm})(x_m - x_{m0})^n, \tag{12}$$

where r is the PML ratio also chosen experimentally. Here, the summation convention is used. The G_l is zero in the region of interest and gradually grows on the interface of the domain and the PML up to values that are typically several orders of magnitude higher than unknown kinematic and stress variables which might make the problem numerically unstable. Fortunately, the governing equations are in the form of $\partial R/\partial t = GR + Q$. As Tabei *et al.*[17] suggested, they can be rearranged in the equivalent representation as $\partial(e^{Gt}R)/\partial t = e^{Gt}Q$ which is a more stable form for numerical implementation

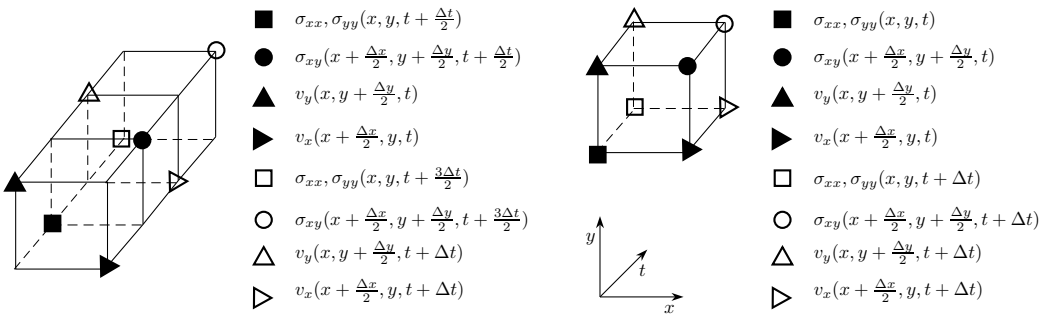

Fig. 1: Staggered grids: Temporal and spatial staggering (right), spatial staggering only (left)

$$\frac{\partial \left(e^{G_l t}{}_l \sigma_{mn}\right)}{\partial t} = e^{G_l t}\left[\lambda \delta_{mn} \frac{\partial v_l}{\partial x_l} + \mu\left(\delta_{nl}\frac{\partial v_m}{\partial x_l} + \delta_{ml}\frac{\partial v_n}{\partial x_l}\right) - \lambda \delta_{mn} v_{0l}\frac{\partial}{\partial x_l}\left(\frac{\sigma_{mn}}{\lambda}\right)\right], \quad (13)$$

$$\frac{\partial \left(e^{G_l t}{}_l v_m\right)}{\partial t} = e^{G_l t}\left[\frac{1}{\rho}\frac{\partial \sigma_{lm}}{\partial x_l} + \frac{1}{\rho}\delta_{lm} f_m - v_{0l}\frac{\partial v_m}{\partial x_l} - v_m \frac{\partial v_{0m}}{\partial x_l}\right]. \quad (14)$$

3.3. *Staggered grids and temporal finite difference schemes*

Stability and efficiency of PSTD methods can be improved by introducing staggered grids as in Ref. [3] and [12]. For all calculations the spatial staggering was implemented such that the velocity and the stress components are evaluated on grids shifted by half of the grid spacing $\Delta x/2$ which modifies the spatial derivative (6) as

$$\frac{\partial [.]}{\partial x^{\pm}} \approx Re\left(\mathcal{F}^{-1}\left(ike^{i\pm \Delta x/2}\mathcal{F}(.)\right)\right). \quad (15)$$

Temporal staggering was additionally implemented for cases of zero background flow and equations were integrated with explicit leap-frog finite difference scheme. For the remaining cases convective terms on the right hand side of (13), (14) introduce same unknowns as those associated with the time derivative. In the other words, the equations are not interlaced any more which is a necessary requirement for temporal staggering[18] and in such case AB3 scheme was implemented instead. A schematic representation of the staggered grids we have employed are shown in Figure 1.

4. Test cases

In this section we present two numerical verifications of the proposed method in two spatial dimensions. The test cases have been chosen such that effects of the temporal staggering, background flow and different time integration schemes can be discussed.

4.1. *Test case 1: Point source in unbounded homogeneous elastic medium*

In this example we consider a point source in an infinite homogeneous quiescent medium. A similar comparison was done by Firouzi *et al.*[12] for the k-space model. The domain is a square $[-20, 20]$x$[-20, 20]$ mm with the compressional sound velocity $c_p = 1500$ m.s^{-1}, shear velocity $c_s = 750$ m.s^{-1} and the mass density of $\rho = 1000$ kg.m^{-3}. The Courant-Friedrichs-Lewy number is set to $CFL = \frac{\max(c_p, c_s)\Delta x}{\Delta t} = 0.2$. The source is located in the center of the domain $\mathbf{x}_s = (0, 0)$ mm and a receiver is located at $\mathbf{x}_r = (0, 10)$ mm. We use the Ricker wavelet as an explosive source

$$f(t) = f_x = f_y = \left(1 - 2\pi^2 f_c^2 (t - t_d)^2\right) e^{-\pi^2 f_c^2 (t-t_d)^2}, \tag{16}$$

with center frequency $f_c = 0.6$ MHz and time delay $t_d = \frac{3f_c}{2}$. As there is no background flow in this case the temporal staggering can be implemented. Performance of Central Euler, Leap frog and 3rd order Adams-Bashforth finite difference schemes is examined by comparison with an analytical solution that was evaluated by numerically convolving Green's function[19].

The relative L_2 error as a function of PPMW is depicted in Figure 2 and a significant improvement is observed for the central Euler when time-staggered meshes are used and the relative error is below 0.5% already for PPMW ≈ 3.9. The Adams-Bashforth without the time-staggering performs equally well and even though it requires more memory than the other two methods it can be used for background flow cases and was therefore implemented in the rest of this work. Figure 3 represents comparison between the analytical solution and the proposed method with the AB3 used for time integration that show a good agreement.

4.2. *Test case 2: Point source in a uniform mean flow*

In this example we consider a point source in an infinite homogeneous acoustic medium with constant background flow with only v_{0x} component being non-zero. The explosive source, the domain and the CFL is the same as in the previous test case. The sound velocities are $c_p = 1500$ m.s^{-1}, $c_s = 0$ m.s^{-1}, Mach number $M = \frac{v_{0x}}{c_p} = 0.2$ and the mass density is $\rho = 1000$ kg.m^{-3}. The temporal staggering was not implemented due to the difficulties discussed in the previous section and AB3 method was therefore used.

Figure 4 represents comparison of the method and analytical solution given by Watanabe[20], this time as a snapshot for $y = 0$ mm at $t = 10$ μs. The curves are in a good agreement and, as expected, the wave gets compressed/elongated as it propagates against/with the flow.

It is generally known that convective terms can pose some stability and dispersion error issues when using an explicit time integration scheme[21]. Using the method of frozen coefficients[10] it can be shown that all eigenvalues λ_{eig} of the system (1), (2) discretized with the Fourier collocation method are imaginary. Presence of the background flow v_{0k} introduces non-zero real parts to the eigenvalues and this is the reason why Central Euler cannot be used as its stability region in the $\lambda_{eig}(\Delta t)$ plane is an open imaginary interval. The choice of the AB3 method was based on the fact that its stability region encloses a

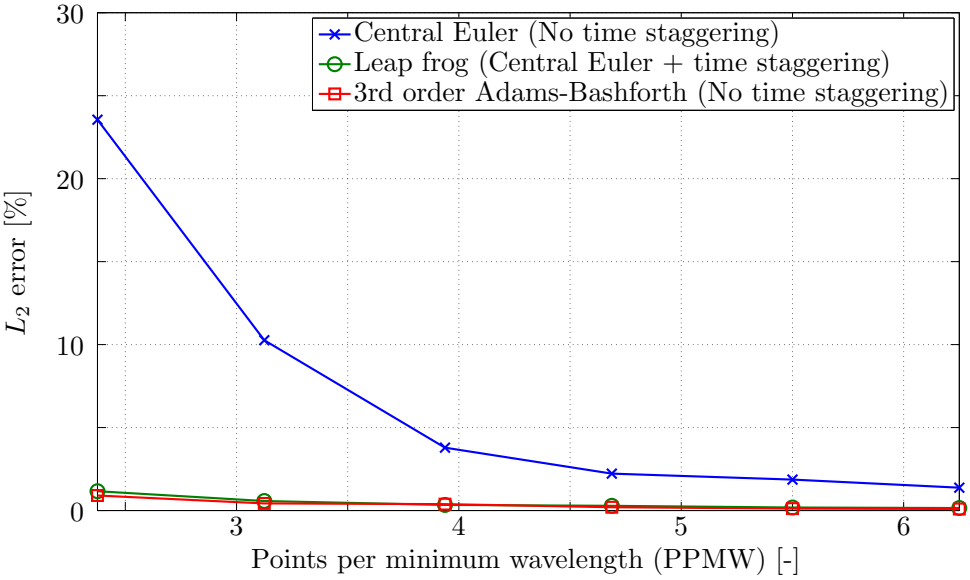

Fig. 2: Comparison of accuracy of PSTD method for different time integration schemes

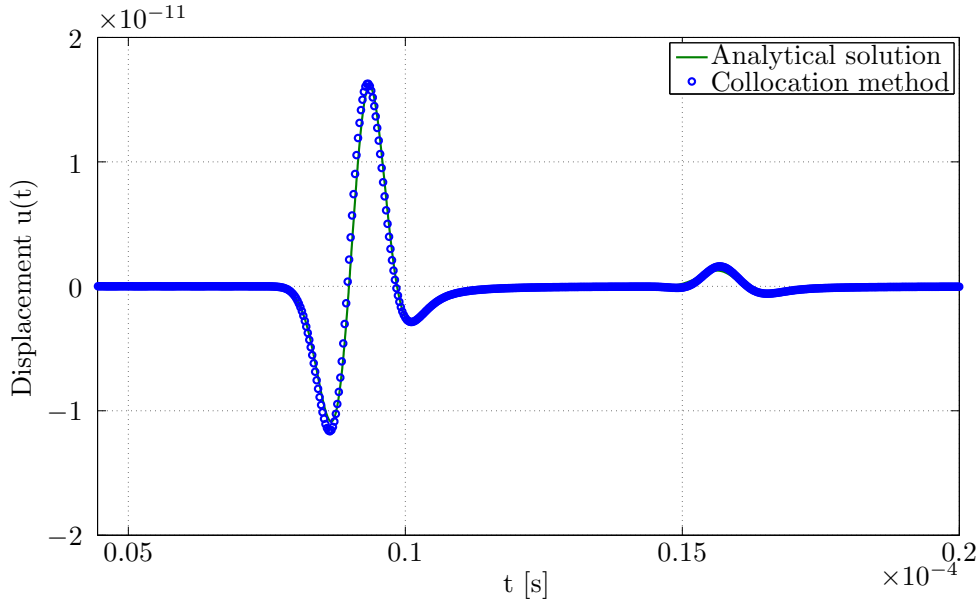

Fig. 3: Comparison of PSTD method and analytical solution at $\mathbf{x}_r = (0, 10)$ mm, test case 1

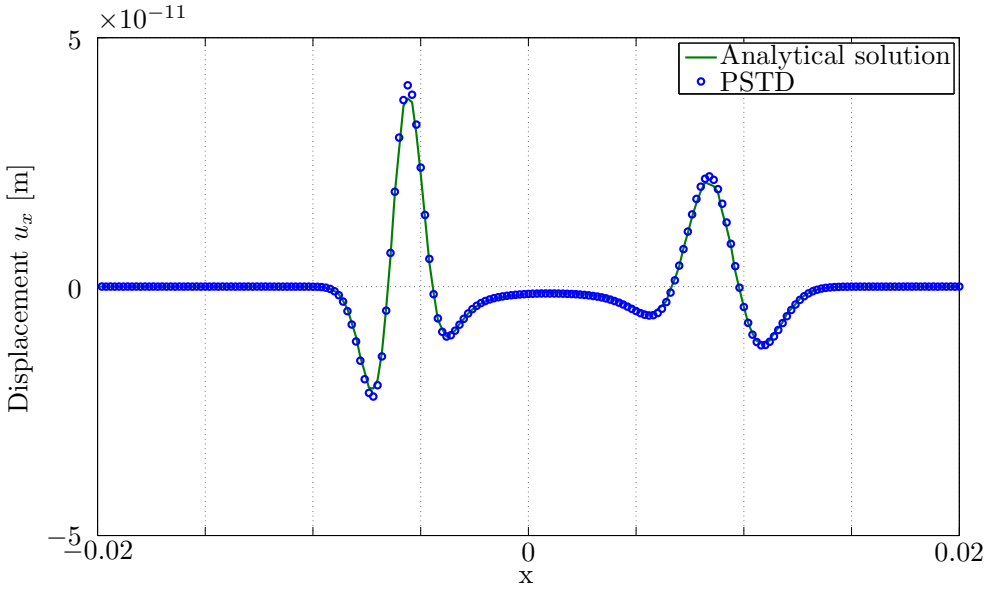

Fig. 4: Comparison of PSTD method and analytical solution at $y = 0$ mm, $t = 10$ μs, test case 2

neighbourhood of the imaginary axis. There was no explicit stability condition found but numerical experiments did not reveal any instabilities for $M \leq 0.5$ and $CFL \leq 0.3$ when propagating a wave packet over a distance of 100 wavelengths which is well within the limits of the presented study. Secondly, the AB3 method was checked for the numerical dispersion. Following the same procedure as Tam[21] the normalized group velocity error c_{error} as a function of $2\pi f \Delta t$ where f is the frequency is presented in Figure 5. In all simulations in this work, the spatial discretization Δx is calculated based on the desired PPMW value

$$\Delta x = \frac{c_{min}}{\mathrm{PPMW}\, f_c}, \tag{17}$$

where c_{min} is the minimum sound velocity in the domain and f_c is the center frequency of an input signal. Assuming again the propagation distance over 100 wavelengths in a medium with the highest sound velocity in the domain c_{max} and requiring that the trailing waves caused by the dispersion errors should travel less than Δx over such distance gives after some manipulation the constraint

$$c_{error} \leq \frac{c_{min}}{c_{max}} \frac{1}{\mathrm{PPMW100}}. \tag{18}$$

The time step Δt is then always checked to satisfy this condition using the relation given in Figure 5 but it was found that the accuracy requirements pose higher restrictions.

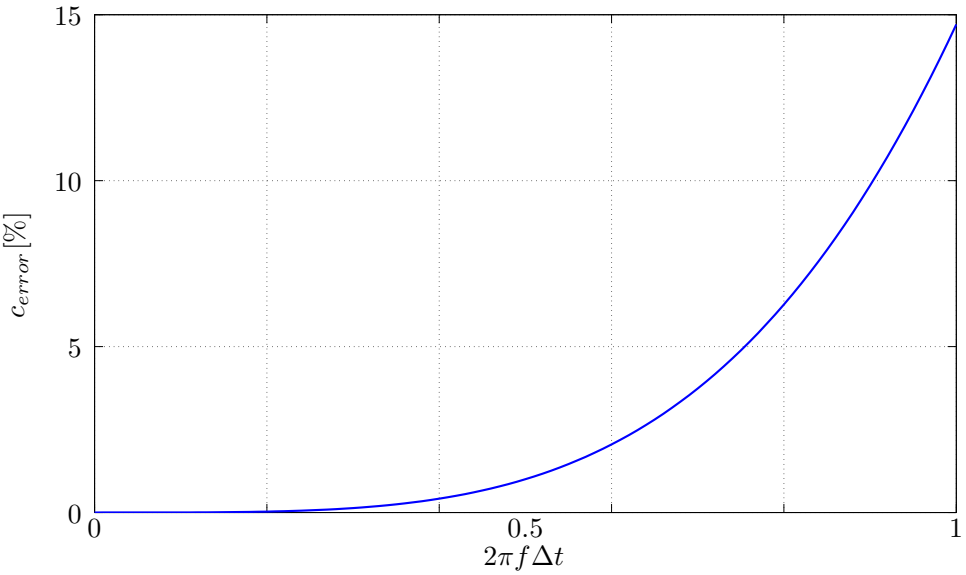

Fig. 5: Normalized group velocity error

5. Clamp-on flowmeter model

In this section we present a full model of a clamp-on transit time ultrasonic flowmeter and discuss how this model is affected by the addition of a flow profile or inhomogeneities to the medium.

5.1. *Impact of the flow profile*

TTUFs calculate the flow based on the transit time difference Δt of signals propagating with and against the flow. As the velocity is typically not the same across the entire cross section the flow is averaged along the path the ultrasonic beam propagates. To compensate for a specific velocity profile the so called *hydraulic factor* k_h[1] is introduced into the equation for calculating the flow[22]

$$\bar{v} = k_h \frac{c_0}{\sin \vartheta_0} \frac{t_{up} - t_{down}}{2t_{f0}}, \tag{19}$$

where t_{up} and t_{down} are the transit times of ultrasonic signals propagating against and with the flow respectively, t_{f0} is the transit time in quiescent fluid, c_0 is the primary wave sound velocity in the coupling wedge and ϑ_0 is the angle of the ultrasonic beam in the wedge with respect to pipe axis. All the parameters are depicted in Figure 6 which represents longitudinal cross section of the center of the pipe.

The equation is derived in the two-dimensional (2-D) description which is an acceptable assumption. The plane transducers and curved pipe wall create a line contact which reduces

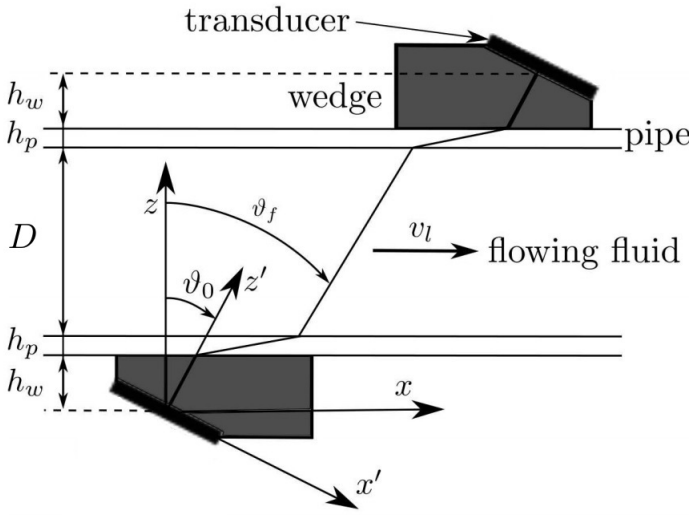

Fig. 6: Scheme of clamp-on TTUF

the received signal amplitude but has nearly no influence on the measurement accuracy[22] which can be demonstrated by numerical analysis[23]. The following case studies are therefore analysed in the 2-D description. Additional assumption that is made when deriving the flow equation (19) is that the transducers generate plane waves which is not true for apertures of finite sizes and the associated error becomes more prominent once the transducers are shifted from their ideal positions as shown by Funck & Mitzkus[22]

We shall present a similar comparison as done by Luca *et al.*[24]. We verify our model for several flow velocities for uniform and power law profile given in Ref. [1]

$$v(r) = v_m \left(1 - \frac{2r}{D}\right)^p, \tag{20}$$

where r is the distance from the pipe axis, p depends on the Reynolds number Re

$$p = 0.25 - 0.023 \log_{10} Re, \tag{21}$$

$$Re = \frac{\bar{v} D}{\mu}, \tag{22}$$

where D is the inner piper diameter, μ is the kinematic viscosity and v_m is the velocity on the pipe axis

$$v_m = v(0) = \bar{v}\,(1+p)\left(1+\frac{p}{2}\right). \tag{23}$$

The uniform flow profile is simulated by simply setting $p = 0$. The pipe is made of steel ($c_p = 5892.5$ m.s^{-1}, $c_s = 3200$ m.s^{-1}, $\rho = 7850$ kg.m^{-3}) filled with water($c_p = 1482$ m.s^{-1}, $c_s = 0$ m.s^{-1}, $\rho = 1024.4$ kg.m^{-3}), has the inner diameter $D = 13.9$ mm, wall thickness $h_p = 3.73$ mm and length 105 mm. Two clamp-on sensors are placed each on one side of the pipe from the distance $h_w = 12$ mm under the angle $\vartheta_0 = 45^o$ (resulting in the angle in the fluid $\vartheta_f \approx 25.5^o$) and aperture size of 15 mm. A typical coupling plastic material ULTEM[25] ($c_p = 2464$ m.s^{-1}, $c_s = 1092$ m.s^{-1}, $\rho = 1280$ kg.m^{-3}) is defined in the entire domain outside of the pipe. This is an acceptable approximation for some transducer designs where the coupling wedge is long enough and the next several signal reflections that have the most impact on the received signal take place on the pipe-wedge interface. The domain is a square $[-52.5, 52.5]$x$[-52.5, 52.5]$ mm discretized in 508x508 elements, $CFL = 0.2$ and the PMLs are implemented so as to avoid wave wrapping issues. The simulation requires approximately 360 MB of memory on a personal computer with quad-core CPU wih 2.6 GHz base frequency. Final time $t_f = 4.7\text{x}10^{-5}$ of one simulation is reached in 9100 s after 6650 iterations. The input signal is a train of eight sine pulses of the frequency $f = 0.77$ MHz multiplied by a Hamming window. The frequency was chosen based on the system configuration with respect to ϑ_0 and the pipe thickness h_p so that a resonance in the pipe wall is achieved resulting in a waveform that is easier to detect on the receiver side as more energy is transmitted making the system robust to noise. A rigorous method how to find harmonics of sandwiched elastic layers was performed by Ainslie[26]. An analogical study related to this topic for inline ultrasonic flowmeters was presented by Willatzen[27] who demonstrated how correct thickness of a material coupled with the piezoceramic element results in received signals with steep front edge. The transit time difference is calculated by cross correlating up- and down-stream received signals and the correlation maximum is approximated by a second order polynomial fit on the three points of the highest correlation values. The received signal used for calculating the measurement error is a pressure normal to the transducer plane σ_n averaged over the aperture width. Transducers are not modelled in this study but it is assumed that two identical piezoceramic elements operating in thickness mode would be normally used. In such case, they can be modelled as linear systems[27] and should have no effect on the measurement error. Two snapshots of the simulation are presented in Figure 7 showing the sonic beam before it enters the pipe (7a) and mode conversion in the pipe wall and radiation into the fluid (7b).

In the first case we assume that the background velocity distribution $v(r)$ is known and the hydraulic factor k_h can be calculated directly as[1]

$$k_h = 1 + \frac{p}{2}. \tag{24}$$

Results of this test are presented in Figure 8 and show low simulated measurement errors below 0.5% which is likely due to numerical errors associated with grid discretization and

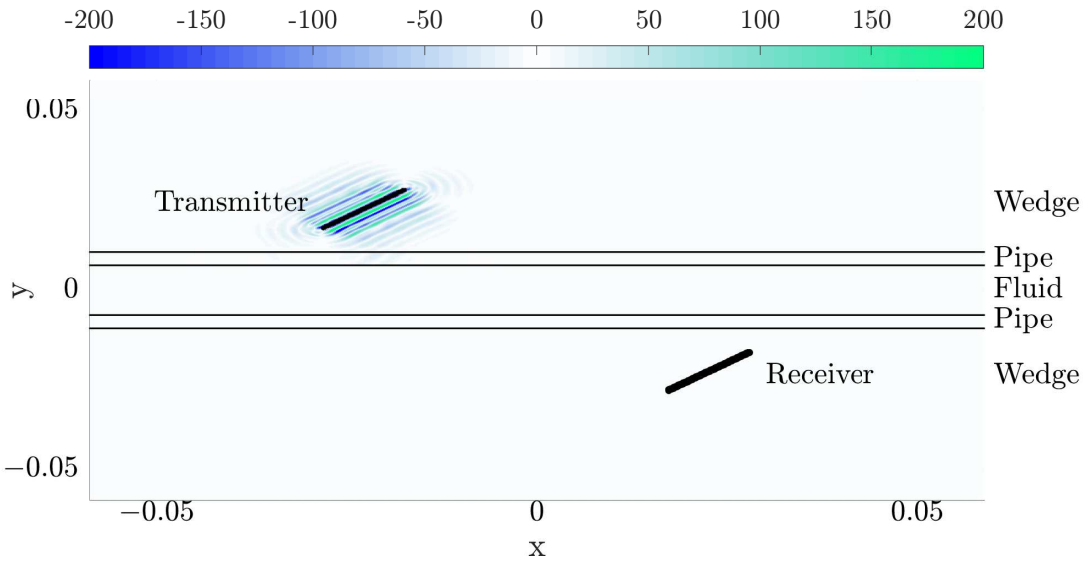

(a) Simulation time $t = 6.5$ μs

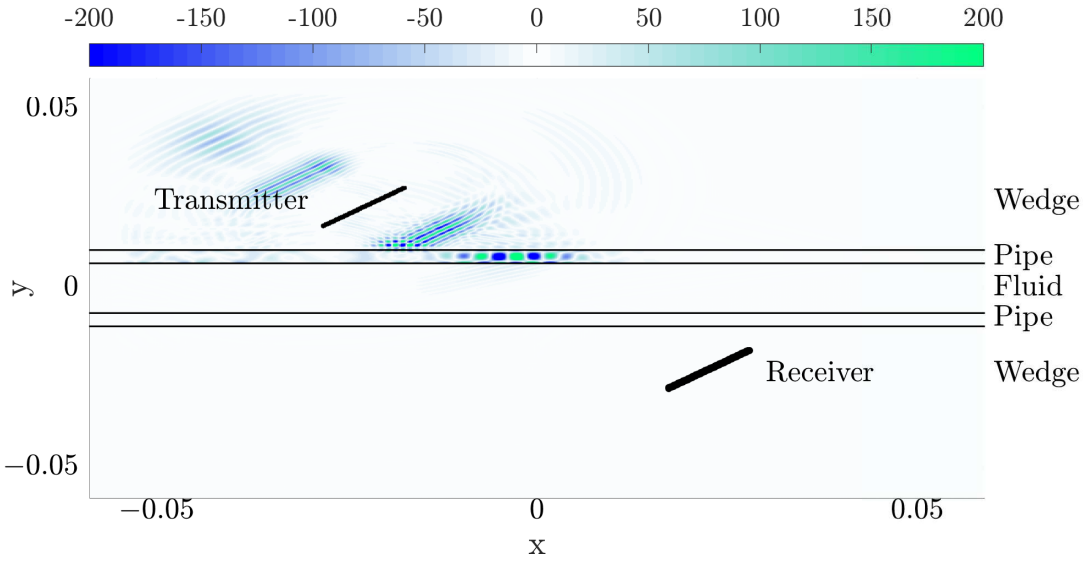

(b) Simulation time $t = 16$ μs

Fig. 7: Simulation snapshots: distribution of the normal pressure σ_{xx}

the fact that the signal does not propagate in form of plane waves as discussed above. The higher error for the power law profile possibly originates from the term $\frac{\partial v_{0i}}{\partial x_k}$ in (5). The flow profile is continuous but not smooth at $r = 0$ for $p \neq 0$ resulting in discontinuity in its first derivative which in turn results in higher truncation errors compared to the uniform profile.

These results represent additional verification of the numerical model but do not mimic

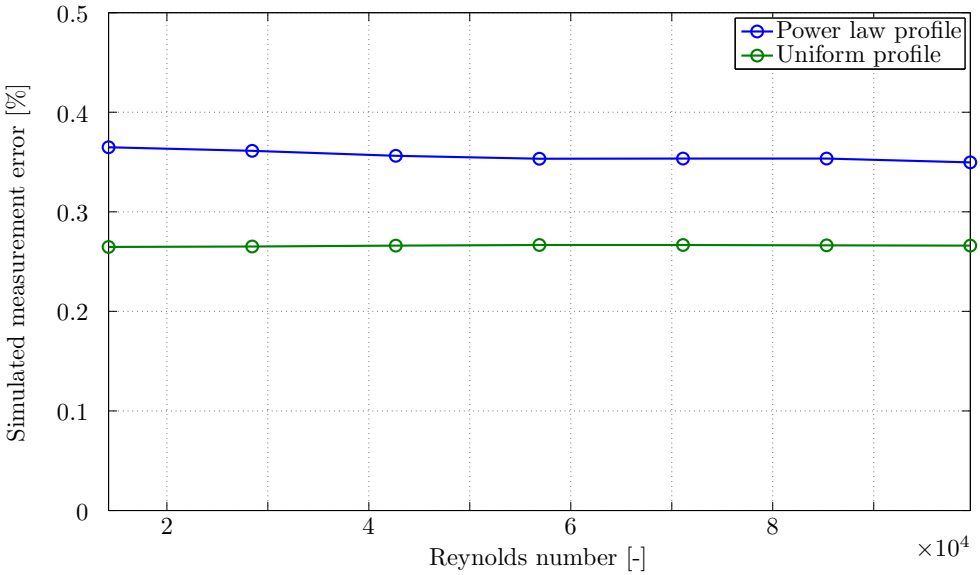

Fig. 8: Simulated measurement errors for a known flow profile

real-life scenarios. In the most typical flow metering application the flow profile is not known and therefore an educated guess needs to be made. The transit times calculated previously were used to calculate Reynolds number and subsequently factor k_h based on the formula given in Ref. [28].

$$k_h = 0.889 + 0.0091 \log_{10} Re + 0.0001 \log_{10}^2 Re, \tag{25}$$

which is an example of practical compensation for variations in flow profile used in commercial flowmeters[29]. The results simulating the situation when the exact background velocity distribution is unknown are presented in Figure 9, showing a significant difference between the measurement errors for the uniform and power law case. The formula for the hydraulic factor is designed for typical flow profiles encountered in practical applications and therefore the power law situation gives much lower measurement error compared to the uniform flow case that is practically very difficult to achieve. Although the high error for uniform flow profile is expected in this scenario an overall message is that a correct flow profile assumption has a significant impact on the measurement error.

5.2. *Impact of flow inclusions*

The flow equation (19) is derived under the assumption of a homogeneous medium. However, in many practical applications flowing media consist of two or more substances. One example is a bubbly flow of gas/liquid mixture. This can affect the received signal significantly depending on the acoustic impedance difference of the inclusions and the surrounding

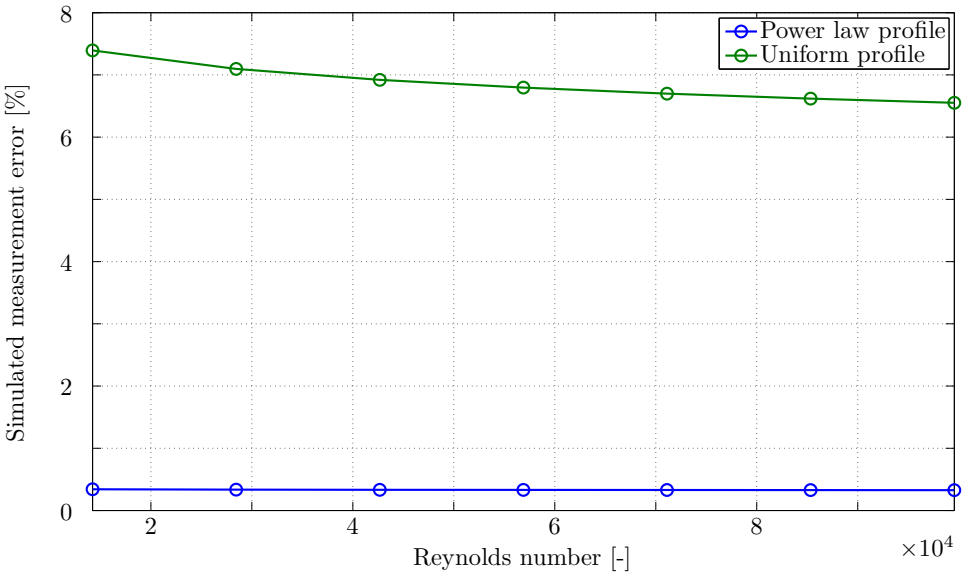

Fig. 9: Simulated measurement errors for an unknown flow profile

medium as well as the inclusion diameter compared to the wavelength of the acoustic signal in the flowing medium. In this study an impact of a single inclusion is investigated. The pipe is again filled with water, has the inner diameter $D = 13.9$ mm, wall thickness $h_p = 3.73$ mm and length 50 mm, wedge height $h_w = 6$ mm, the angle $\vartheta_0 = 45^{\circ}$ and aperture size of 6.1 mm. The domain is a square $[-25, 25]$x$[-25, 25]$ mm discretized in 186x186 elements, $CFL = 0.2$ and the input signal is a train of eight sine pulses of the frequency $f = 0.77$ MHz multiplied by the Hamming window. A circular inclusion was placed in the center of the pipe directly in the sonic path. The inclusion has a diameter d and is considered to be an air bubble but instead of assigning material properties of air at the specific grid nodes an alternative approach was taken by directly imposing zero values on stress variables at each stage of the time integration[a], resulting in total reflection on the boundary which is an acceptable approximation considering high air/water impedance mismatch. This way we avoid numerical issues that would be associated with a spectral differentiation of mass density.

The results presented in Figure 10 show received signals for various inclusion diameters. For the given frequency of the input signal the width of the acoustical wave-front in water is approximately 11 mm. As expected the signal gets attenuated with growing inclusion size but more importantly the envelope changes its shape for greater diameters and the signal gets more wide-banded which can be clearly seen from the frequency spectrum of

[a]In case of quiescent media ($v_{0k} = 0$), imposing zero values on stress is identical to setting Lamé parameters to zero

the signals shown in Figure 11. This can cause problems in the real flow measurement application where upstream and downstream received signals under bubbly flow regime are typically not captured at the very same moment. One can think of a scenario in which one signal propagates through clean fluid while the other one faces a bubble. These different conditions violate the reciprocity of the system and the envelope distortion can result in a faulty calculation of the transit time difference if signals are not correlated properly.

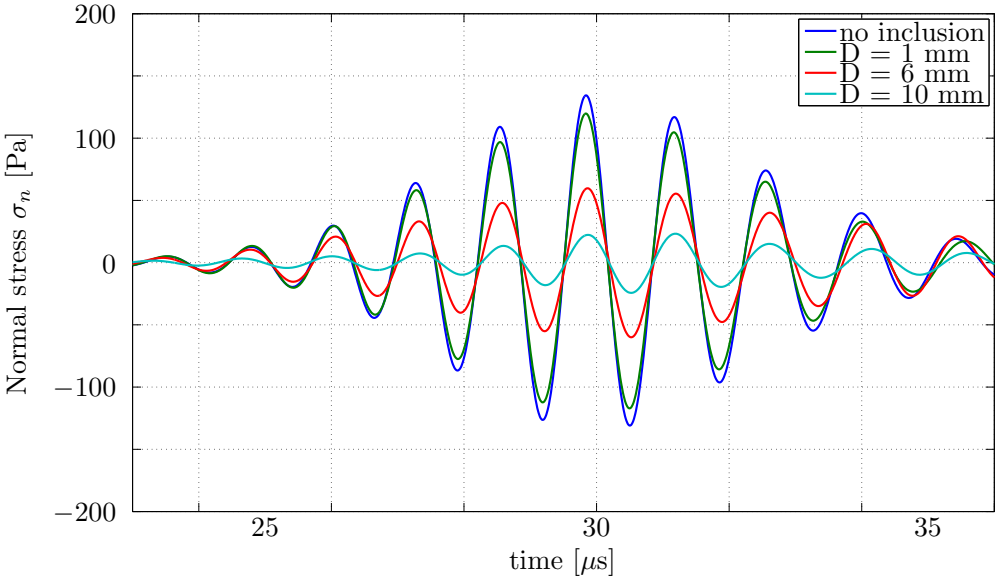

Fig. 10: Impact of the inclusion size on the received signal

and limits of effective media approaches

6. Conclusion

A goal of this work was to create a model able to simulate a clamp-on ultrasonic flow meter under various sorts of flow conditions. For that purpose the PSTD method solving the equations of linear elasticity with background flow was developed. The method was validated against analytical solutions showing good agreement and superior performance with respect to required PPMW compared to other numerical approaches. The study of flow profile influence confirmed the necessity of proper utilisation of hydraulic factor to avoid false flow rate readings and promising performance capabilities were shown for analyzing more complicated two-phase flow, with the possibility to analyze attenuation by bubbles. The method revealed that received waveform can become significantly distorted violating the assumption of reciprocity of upstream and downstream received signals. Great care must be taken when calculating difference of transit times in such situations. The current

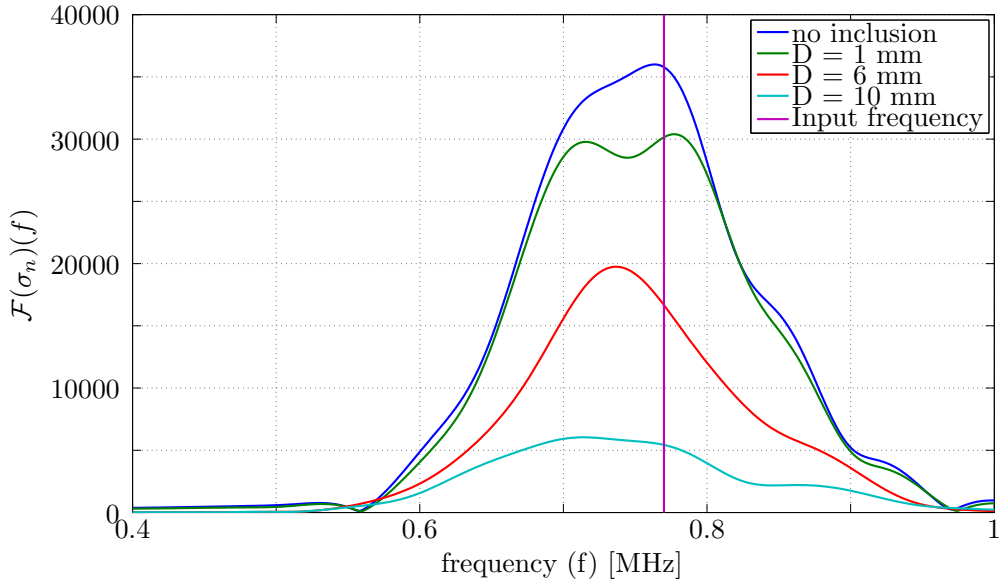

Fig. 11: Frequency spectrum of received signals for different inclusion sizes

formulation doesn't employ any attenuation mechanisms and further studies considering clusters of inhomogeneities as well as comparison against real measurements should be performed. Additionally, situations where frequency of the input signal is close to harmonics of the second phase inclusions or when acoustic impedance of the second phase is closer to the ambient medium should be investigated. This is a subject to future work.

References

1. B. Iooss, C. Lhuillier and H. Jeanneau, Numerical simulation of transit-time ultrasonic flowmeters: uncertainties due to flow profile and fluid turbulence, *Ultrasonics* **40** (2002) 1009-1015.
2. H. Koechner and A. Mellin, Numerical Simulation of Ultrasonic Flowmeters, *Acustica-acta acustica* **86** (2000) 39-48.
3. B. Fornberg, High-order finite differences and the pseudospectral method on staggered grids, *SIAM J. Numer. Anal.* **27** (1990) 904-918.
4. D. V. Mahadeva and R. C. Baker and J. Woodhouse, Studies of the Accuracy of Clamp-on Transit Time Ultrasonic Flowmeters, *IMTC IEEE* (May 2008) 969-973.
5. M. Bezdek and H. Landes and A. Rieder and R. Lerch, A coupled finite-element, boundary-integral method for simulating ultrasonic flowmeters, *IEEE UFFC* **54** (2007) 639-646.
6. Q. H. Liu, The PSTD algorithm: A time-domain method requiring only two cells per wavelength, *Microwave and Optical Technology Letters* **15** (1997) 158-165. Q. H. Liu
7. B. A. Auld, *Acoustic Fields and Waves in Solids, Vol. I.* (John Wiley & Sons, 1973).
8. R. J. LeVeque, *Finite Difference Methods for Ordinary and Partial Differential Equations: Steady-State and Time-Dependent Problems* (SIAM, 2007).
9. A. D. Pierce, Wave equation for sound in fluids with unsteady inhomogeneous flow, *J. Acoust. Soc. Am. Vol.* **87** (1990) 2292-2299.

10. L. N. Trefethen, *Spectral Methods in MATLAB* (SIAM, 2001).
11. B. Fornberg, *A Practical Guide to Pseudospectral Methods* (Cambridge University Press, 1996).
12. K. Firouzi, B. T. Cox, B. E. Treeby and N. Saffari, A first-order k-space model for elastic wave propagation in heterogeneous media, *J. Acoust. Soc. Amer.* **132** (2012) 1271-1283.
13. F. D. Hastings, J. B. Schneider, and S. L. Broschat, Application of the perfectly matched layer (PML) absorbing boundary condition to elastic wave propagation, *J. Acoust. Soc. Am. Vol.* **100** (1996) 3061-3069.
14. J.S. Hesthaven, J. Métral, O. Vacus, On the Analysis and Construction of Perfectly Matched Layers for the Linearized Euler Equations, *Journal of Computation Physics* **142** (1998) 129-147.
15. J.L. Lions, J. Métral, O. Vacus, Well-posed absorbing layer for hyperbolic problems, *Numerische Mathematik* **92** (2002) 535-562.
16. K. C. Meza-Fajardo, A. S. Papageorgiou, A Nonconvolutional, Split-Field, Perfectly Matched Layer for Wave Propagation in Isotropic and Anisotropic Elastic Media: Stability Analysis, *Bulletin of the Seismological Society of America* **98** (2008) 1811-1836.
17. M. Tabei, T. D. Mast, and R. C. Waag, A k-space method for coupled first-order acoustic propagation equations, *J. Acoust. Soc. Am. Vol.* **111** (2002) 53-63.
18. M. Ghrist, B. Fornberg and T. A. Driscoll, Staggered Time Integrators For Wave Equations, *SIAM J. Numer. Anal.* **38** (2000) 718-741.
19. E. Kausel, *Fundamental Solutions in Elastodynamics: A Compendium* (Cambridge University Press, New York, 2006).
20. K. Watanabe, *Integral Transform Techniques for Green's Function, Lecture Notes in Applied and Computational Mechanics* **71** (Springer 2014).
21. C. K. W. Tam, *Computational Aeroacoustics: A Wave Number Approach* (Cambridge University Press, Cambridge, 2014).
22. B. Funck, A. Mitzkus, Acoustic transfer function of the clamp-on flowmeter , *IEEE UFFC* **43** (1996) 569-575.
23. B. Funck, Akustische Clamp-on-Messtrecke, *Ph.D. dissertation* **111** Univ. Rostock (1995).
24. A. Luca, R. Marchiano, J.-C. Chassaing, A Discontinuous Galerkin Approach for the Numerical Simulation of Transit-Time Ultrasonic Flowmeters, *IUS, IEEE International* (2014) 935-938.
25. ULTEM^{TM} Resin All series. *http://www.sabic-ip.com/gepapp/Plastics/servlet/ProductsAndServices/Product/series?sltPrdline=ULTEM& search=Search# searchresults*, September 2015
26. M.A. Ainslie, Plane-wave reflection and transmission coefficients for a three-layered elastic medium, *J. Acoust. Soc. Am. Vol.* **97** (1995) 954-961.
27. M. Willatzen, Ultrasound transducer modeling-general theory and applications to ultrasound reciprocal systems, *IEEE UFFC* **48** (2001) 100-112.
28. K.S. Mylvaganam, High-Rangeability Ultrasonic Gas Flowmeter for Monitoring Flare Gas, *IEEE TUFFC Vol.* **36** (1989) 144-149.
29. K.S. Mylvaganam, T. Folkestad and R.No, Fluenta FGM 100 ultrasonic fas flowmeter, *CMI-no. 871413-1* Bergen, Norway (1989).